Available online at www.sciencedirect.com
ScienceDirect
Applied Catalysis B: Environmental 80 (2008) 147–155
APPLIED CATALYSIS B: ENVIRONMENTAL
www.elsevier.com/locate/apcatb

Bimodal mesoporous TiO_2–P25 composite thick films with high photocatalytic activity and improved structural integrity

Yongjun Chen, Dionysios D. Dionysiou *

Department of Civil and Environmental Engineering, University of Cincinnati, Cincinnati, OH 45221-0071, USA

Received 6 April 2007; received in revised form 15 October 2007; accepted 14 November 2007
Available online 22 November 2007

Abstract

Bimodal mesoporous TiO_2–P25 composite thick films with improved structural integrity (less crack formation) were successfully synthesized by employing an environmental friendly and highly viscous nonionic surfactant Tween 20 as a tri-functional template, which can simultaneously improve film texture, bimodal mesopore structure and structural integrity in the films. It was found that increasing Tween 20 loading from 10% to 50% (v/v) could simultaneously increase both volumes of small mesopore and secondary large mesopore. Degussa P25 nanoparticle can function as a kind of pore wall contributing to the formation of secondary large mesopore. Optimizing the loading of Tween 20 could result in optimum film thickness, even with only one dip-coating cycle. The final film at optimum Tween 20 loading (50%, v/v) exhibited large porosity (50.6%) and bimodal mesoporous size distribution with small mesopore size of ~5 nm and large mesopore size of ~34 nm. Compared with mono-modal mesoporous TiO_2 film (no Degussa P25) at optimum preparation conditions (Tween 20, 50% (v/v), six dip-coating layers), the TiO_2–P25 composite films prepared with the same Tween 20 loading (one dip-coating layer) or with 25% (v/v) Tween 20 loading (two dip-coating layers) demonstrated higher photocatalytic activities in the degradation of creatinine, an important human metabolite present in human urine. These results prove that bimodal mesoporous TiO_2–P25 composite films have promising properties for photocatalytic water treatment.

Keywords: Surfactant; Tween 20; Self-assembling; Sol–gel; TiO_2; P25; Photocatalysis; Films

1. Introduction

Titanium dioxide (TiO_2) has been considered a promising material in applications of environmental photocatalysis and photochemical solar cells [1–20]. To maximize utilization of titanium dioxide photocatalyst for practical industrial applications, it is necessary to develop film (i.e., immobilized on supports) type TiO_2 photocatalysts [10,13,14,16,18–28]. For this reason, preparation of immobilized photocatalytic films has received great attention by scientists and engineers during the last several years [10,13,14,18–28]. It has been well established that the surfactant self-assembling sol–gel method is a promising and popular technology for the synthesis of transparent porous TiO_2 films [22,23,27,28]. However, like other sol–gel-derived TiO_2 films, these porous photocatalytic films often have small film thickness (i.e., 100 nm) at each dip-coating cycle [27], which does not yield to optimum photocatalytic activity due to the small amount of crystalline material and not optimum UV light utilization across the film [19,29]. Increasing the number of dip-coating cycles can achieve optimum film thickness and enhanced photocatalytic activity. However, this procedure has some deficiencies such as the requirement for a large number of dip-coating cycles and limited improvement in film photocatalytic activity due to non-optimum pore structure (i.e., compaction of the inner film layers during successive calcination cycles). More recently, it has been demonstrated that the film thickness can be remarkably increased by incorporating suitable amounts of Degussa P25 nanoparticles into the precursor sol [13,14,20,21,26,30,31]. However, for thicker films, when the pore size is not large enough (i.e., micropores or small mesopores), mass transfer limitations between the treated contaminant molecules and active catalytic sites in the inner layers of the films may be a more serious problem. Therefore, it is important to design a well-defined pore structure to improve mass transfer of the treated contaminant molecules in the inner pore channels of the thicker films.

* Corresponding author.
E-mail address: dionysios.d.dionysiou@uc.edu (D.D. Dionysiou).

0926-3373/$ – see front matter © 2007 Elsevier B.V. All rights reserved.
doi:10.1016/j.apcatb.2007.11.010

Design of a well-defined pore structure is in fact an important topic in the synthesis of inorganic materials for various applications [32–37] since the pore structure, including porosity and pore size distribution, has great effect on the activity of photocatalytic materials [9,25]. Currently, the preparation of high surface area porous inorganic materials as supports or catalysts with bimodal pore size distribution is an active area of research in the field of heterogeneous catalysis. This is because the small pores (i.e., micropores or small mesopores) contribute a large area of active surface for strong interaction of adsorbed molecules to the active sites whereas the large pores (i.e., macropores or larger mesopores) provide the channels for fast intraparticle molecular transfer [32,34,35,38,39].

Recently, we successfully developed a porous TiO_2–P25 composite film with meso–macropore bimodal pore structure by optimizing the calcination temperature [25]. It was suggested that, although the P25 loading in the sol is relatively low (10 g/L) (i.e., compared to 30 and 50 g/L), this film did not experience a serious problem with cracks and its photocatalytic activity was comparable to those of the films synthesized at high P25 loading. It is believed that both advantages are associated with the presence of macropores in the film, which can help reduce compressive stress during calcination and facilitate transport of parent contaminants and reaction byproducts within the large pore channels [25].

In this study, motivated by designing a tailor-made bimodal pore structure for TiO_2–P25 composite films, we employed a nonionic surfactant Tween 20 as pore-directing agent in the P25 powder-modified sol. It was found that TiO_2–P25 composite films with high BET surface area/porosity, bimodal pore structure, and improved structural integrity could be synthesized by this method.

2. Experimental

2.1. Preparation of mesoporous TiO_2 films and mesoporous TiO_2–P25 composite films

Commercial ultrapure titanium isopropoxide (TTIP, 97%, Aldrich), 1-butanol (anhydrous, 99.8%, Aldrich,) and acetylacetone (99%, Fisher Scientific) were used as precursor materials. First, 1-butanol sol was prepared, which included acetylacetone (0.28 M), TTIP (0.46 M), H_2O (0.92 M) and 1-butanol solvent. Then, Tween 20 and 1-butanol solvent were added to the butanol sol at different volume ratios, which are summarized in Table 1. For the synthesis of TiO_2–P25 composite films, a modified 1-butanol sol containing 10 g/L Degussa P25 was used instead of a plain 1-butanol sol. The procedure for the preparation of P25 powder-modified sol is similar to that of former publications [21,25,26]. In addition, while the samples are prepared, the P25 powder-modified sol is treated using ultrasonic cleaner (model number B200, Cole-Parmer) for 3 min, so as to improve the dispersion of the P25 nanoparticles in the sol.

The dip-coating apparatus and high temperature furnace are the same as those described in our former publications [19,25,26]. A constant withdrawal velocity of 12.3 ± 0.5 cm min^{-1} was employed for the dip coating of the borosilicate glass substrate into the sol. The furnace temperature was incremented at a ramp rate of 15 °C min^{-1} until 100 °C; this temperature was held for 15 min. The temperature of the oven was subsequently increased at a ramp rate of 15 °C min^{-1} to 500 °C and was held at this value for 15 min. Finally, the films were cooled naturally to room temperature.

2.2. Film characterization

The crystal phase composition of the TiO_2 particles and photocatalytic films coated on borosilicate glass was determined by X-ray diffraction (XRD) using a Siemens Kristalloflex D500 diffractometer with Cu Kα radiation. Film morphology was characterized by scanning electron microscopy (SEM; Hitachi S-4000). Element composition of the films was analyzed by energy dispersive X-ray spectroscope (EDX, Oxford Isis). AFM analysis was performed using a Nanosurf® EasyScan 2 AFM model; the samples were scanned by the dynamic and non-contact mode.

Micromeritics TriStar 3000 Gas Adsorption Analyzer was employed for the analysis of BET surface area and pore structure of these photocatalytic films. TiO_2–P25 particle samples are prepared by scraping the TiO_2–P25 films from the borosilicate glass. All particle samples were degassed at 180 °C for 150 min before N_2 adsorption analysis. UV–vis spectra of the photocatalytic films were obtained using a UV–vis spectrophotometer (Hewlett Packard 8452A).

The crystal size and crystal structure of TiO_2 particles was determined by a JEM-2010F (JEOL) high resolution-

Table 1
Compositions of various sols used in the study

P25 powder-modified sol	Degussa P25 concentration (g/L)	1-Butanol sol volume (mL)	Tween 20 volume (mL)	1-Butanol volume (mL)	Final precursor sol volume (mL)	Tween 20/precursor sol (v/v)
P25–Bu sol[a]	10	5.0	0	5.0	10.0	0
P25–1.0T20Bu sol[b]	10	5.0	1.0	4.0	10.0	1:10
P25–2.5T20Bu sol[c]	10	5.0	2.5	2.5	10.0	1:4
P25–5.0T20Bu sol[d]	10	5.0	5.0	0	10.0	1:2

[a] P25–Bu sol: the final sol without Tween 20, 10 g/L P25 powders.
[b] P25–1.0T20Bu sol: 1.0 mL Tween 20 in 10 mL final sol, 10 g/L P25 powder.
[c] P25–2.5T20Bu sol: 2.5 mL Tween 20 in 10 mL final sol, 10 g/L P25 powder.
[d] P25–5.0T20Bu sol: 5.0 mL Tween 20 in 10 mL final sol, 10 g/L P25 powder.

transmission electron microscope (HR-TEM) with field emission gun at 200 kV. Samples were dispersed in methanol (HPLC grade, Pharmco) using an ultrasonic cleaner (2510R-DH, Bransonic) for 5 min and fixed on a carbon-coated copper grid (LC200-Cu, EMS). The strength of adhesion of the TiO_2 films was measured by the crosshatch adhesion test (ASTM D3359B-02 [40]). The cut samples were also examined by a microscope (The Buehler VersaMet®3 metallograph, USA).

2.3. Evaluation of photocatalytic activity of the films

The photocatalytic activity of the TiO_2 films was evaluated using aqueous solution of creatinine (99.5%, Aldrich) with an initial concentration of approximately 19.5 mg/L. The initial volume of creatinine solution was 8 ml. The initial pH of the solution was approximately 6.1. The photocatalytic reactor used was a round borosilicate dish with inside diameter of 4.7 cm. The dimensions of the coatings dipped into creatinine solution were 4.2 cm (length) × 2.5 cm (width). The UV source consisted of two 15 W integrally filtered low-pressure mercury UV tubes (Spectronic Corp., Westbury, NY) emitting radiation with wavelength in the range 300–400 nm and a peak at 365 nm. The average intensity of the UV radiation for each tube measured on the top of the films with covered borosilicate glass cap was approximately 1025 μW/cm^2, which was measured by a UV radiation meter (1L 1700 International Light, Serial No. 2547). The distance between the lamps and the films was less than 1 cm. The reactor was cooled by a fan (Duracraft Corporation, South Borough, MA) positioned near the reactor. Creatinine samples were analyzed using HPLC (Agilent 1100 series) equipped with a diode array detector (DAD) and an auto sampler. The stationery phase used was a 3.9 mm × 150 mm 5 μm NovaPak C18 column (Waters). The mobile phase composition was ammonium sulfate (0.045 M) at a flow rate of 0.320 mL/min. This analysis method was originally developed by Dash and Sawhney [41], and then modified by Antoniou et al. [42].

3. Results and discussion

3.1. Film crystalline composition and thickness

Fig. 1(a) shows XRD spectra of TiO_2–P25 composite films. An obvious diffraction peak at 25.4° of 2θ angle can be observed in all films, which corresponds to anatase (1 0 1). The peak corresponding to rutile phase (i.e., rutile TiO_2 in the (1 1 0) plane) cannot be clearly seen due to small amount of P25 loading in the films. Increasing Tween 20 loading in the sol can remarkably enhance the peak height of anatase phase (1 0 1), which relates to an increased amount of crystalline material. In addition, increasing Tween 20 loading in the sol leads to an enhancement of the full width at half-maximum intensity (FWHM), which is associated with a decrease in the average crystalline size. Because the presence of Tween 20 cannot affect the size of P25 primary nanoparticles in the sol, the decreased average crystal size in the TiO_2–P25 composite films should be mainly attributed to the decreased crystal size of TiO_2 matrix formed from TTIP hydrolysis and condensation. Fig. 1(b) shows XRD spectra of TiO_2 powder samples prepared using the "control" sol (absence of P25 nanoparticles), which were prepared at the same preparation conditions as the TiO_2–P25 composite films (i.e., 500 °C, 15 min). It can be clearly seen that all particle samples present anatase phase without rutile and brookite phases. Increase in the content of Tween 20 results in an increase in the FWHM of the peak intensity at anatase (1 0 1) indicating a decrease in crystal size of the TiO_2 matrix, which is in agreement with our former report [17]. The average crystal sizes of the TiO_2–P25 composite films are presented in Table 2. The average crystal size in TiO_2–P25 composite film decreased to 11.8 nm when Tween 20 loading increased to 50% (v/v). Therefore, from the above results, it can be concluded that the amount of crystalline materials and the average crystal size of TiO_2–P25 composite films can be controlled by simply adjusting the Tween 20 loading in the P25 powder-modified sol (10 g/L P25). Decreased crystal size induced by Tween 20 has also been reported in an acetic acid associated sol–gel process [27]. Hydrolysis and condensation of TTIP leads to the formation of Ti–O–Ti network, which can

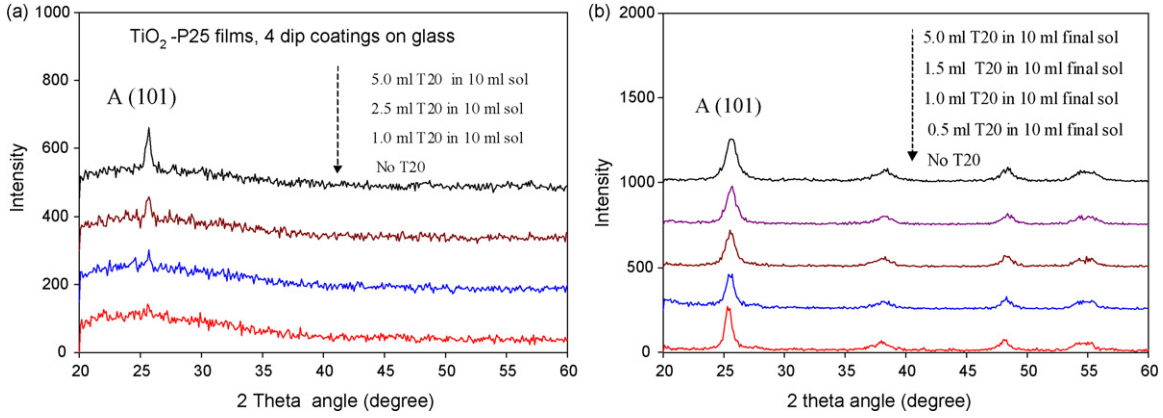

Fig. 1. XRD spectra of photocatalysts. (a) TiO_2–P25 composite films with different Tween 20 loadings (four dip-coating layers) and (b) TiO_2 particles without P25 nanoparticles addition (one time heating cycle).

Table 2
Effect of Tween 20 loading in the sol on the texture, film thickness and photocatalytic activity of TiO_2–P25 composite films

Film	Tween 20 volume (mL) in 10 mL final sol[a]	BET (m^2/g)	Pore volume[b] (cm^3/g)	Pore size[c] (nm)	Porosity[d] (%)	Film thickness per layer (nm)	Crystal size (nm)	Creatinine degradation (%)
5.0T20Bu[e]	5.0	118.8	0.1528	5.2	37.3	182[f]	5–8[g]	77.7 ± 3.8[h]
P25–Bu[i]	0	36.3	0.1084	10.4	29.7	148[j]	17[k], 35[l]	59 ± 3.5[m]
P25–1.0T20Bu[n]	1.0	45.9	0.1698	13.3	39.8	187[j]	21.3[o]	79 ± 2.0[m]
P25–2.5T20Bu[p]	2.5	64.1	0.1949	10.9	43.2	431[j]	14.2[o]	85.8 ± 3.7[m]
P25–5.0T20Bu[q]	5.0	73.7	0.2625	12.2	50.6	525[j]	11.8[o]	89.3 ± 3.2[r]

[a] The total volume of the final sol is considered to be the sum of the volume of 1-butanl sol + the volume of 1-butanol solvent + the volume of Tween 20.
[b] BJH adsorption cumulative volume of pores.
[c] BJH adsorption average pore diameter (4 V/A).
[d] Based on pore volume and 3.9 g/m^3 of anatase density. Porosity (%) = pore volume (cm^3/g)/(pore volume (cm^3/g) + solid catalyst volume without pore (cm^3/g)) × 100%; solid catalyst volume without pore (cm^3/g) = 1/density of the solid catalyst volume without pore.
[e] TiO_2 film prepared from the sol with 5 mL Tween 20 in 10 mL final sol (wthout P25 powder addition).
[f] Film thickness obtained from cross-section SEM.
[g] Based on TEM, samples scratched from the ''thick'' coatings.
[h] Creatinine degradation percentage after 150 min reaction, TiO_2 films with six dip-coating layers.
[i] P25 powder-modified film prepared from P25–Bu sol.
[j] Calculation based on pore volume and average film weight with average density of 3.9 g/cm^3. Film thickness = film weight (g) × (pore volume (cm^3/g) + solid catalyst volume without pore (cm^3/g))/area of the coated support (cm^2).
[k] Based on TEM, average size of the smaller particles (the size is below 25 nm).
[l] Based on TEM, average size of the larger particles (the size is above 25 nm).
[m] Creatinine degradation percentage after 150 min reaction, TiO_2–P25 films with two dip-coating layers.
[n] P25 powder-modified film prepared from P25–1.0T20Bu sol.
[o] Based on XRD, using Scherrer equation: $D = 0.9\lambda/(B\cos\theta)$, where $\lambda = 0.154$ nm.
[p] P25 powder-modified film prepared from P25–2.5T20Bu sol.
[q] P25 powder-modified film prepared from P25–5.0T20Bu sol.
[r] Creatinine degradation percentage after 150 min reaction, TiO_2–P25 films with one dip-coating layer (optimum number of dip-coating layers).

serve as nuclei for further particle growth [43]. Particle growth follows Ostwald ripening mechanism [44], during which smaller particles dissolve and precipitate on larger particles. It has been reported that surfactant film can shield soluble Ti species from depositing on the surface of the precursor particles, which can lead to inhibition of particle growth [45]. It is believed that Tween 20 molecules can occupy some surface sites of larger particles that function as sites for nucleation and as a result some smaller particles cannot precipitate on the larger particles. Therefore, Tween 20 at some extent can inhibit particle growth.

Fig. 2 shows the effect of Tween 20 loading on apparent viscosity (a) and film weight (b). Considering that by employing cross-section SEM to determine the film thickness may cause larger error because of the large roughness of this type of films, the film thickness of TiO_2–P25 composite films was calculated based on the porosity and density of anatase phase. These results are also reported in Table 2. It can be clearly seen that increasing Tween 20 loading can increase film weight and thickness. When Tween 20 loading increases to 50% (v/v), the film weight and thickness of the TiO_2–P25 composite film of one dip-coating layer can reach 101 μg/cm^2 and 525 nm, respectively, which are approximately 2.5 times the film weight and 3.5 times the film thickness of TiO_2–P25 composite film without Tween 20 (P25–Bu film). This is attributed to the enhanced apparent viscosity of the P25 powder-modified sol caused by the addition of the highly sticky Tween 20. On the other hand, it was found that addition of 10 g/L P25 nanoparticles into the sol without Tween 20 can cause only a slight enhancement in the apparent viscosity of the sol (data not shown here). However, the viscosity of the P25 powder-modified sol was significantly increased by increasing the content of Tween 20. Considering that (i) increasing the loading of P25 nanoparticles in the sol, which in the absence of Tween 20 leads to crack formation [26], and (ii) the small increase in apparent viscosity of the sol caused by the low (10 g/L) P25 loading can yield TiO_2–P25 composite films with relatively small film thickness, we believe that one good strategy for obtaining thicker films with optimum thickness (i.e., with only a few dip-coating cycles) with respect to photocatalytic activity and without cracks is the addition of an appropriate amount of Tween 20 in the P25 powder-modified sol.

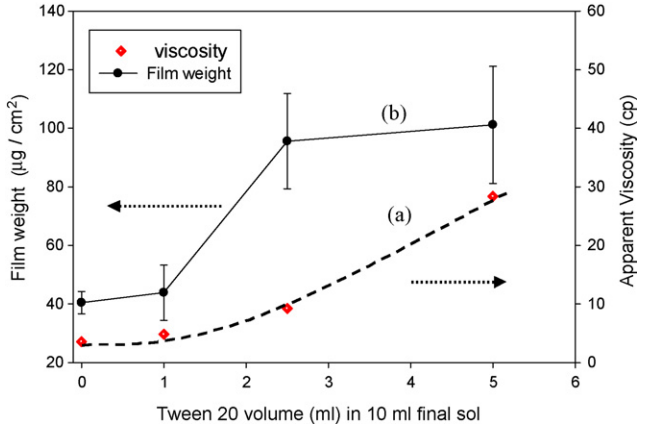

Fig. 2. Effect of Tween 20 loading on apparent viscosity (a) and film weight (b).

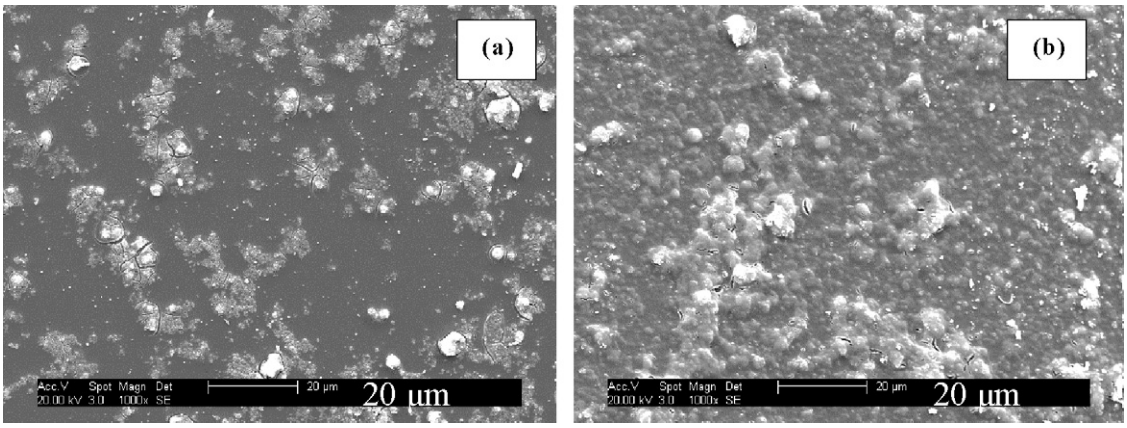

Fig. 3. SEM images of TiO_2–P25 composite films (two dip-coating layers). (a) Without Tween 20 and (b) Tween 20: final sol = 1:2 (v/v).

3.2. Surface morphology and adhesion

Considering that formation of large-size P25 aggregates can lead to crack formation [26], which may have detrimental effect on the long-term mechanical stability of such films used in water treatment applications, the extent of particle agglomeration and overall surface morphology of the TiO_2–P25 composite films were examined by SEM. The results are shown in Fig. 3. Similar to previous published studies [14,20,21,25,26], the TiO_2–P25 composite films showed rough surface morphology, which included the presence of aggregates composed of P25 nanoparticles. The images indicate that (i) adding Tween 20 into the precursor sol can improve the dispersion of P25 particles and P25 nano-agglomerates in the films, and (ii) the number of cracks induced due to P25 particle coagulation decreases. In order to further investigate how Tween 20 affects the dispersion of the P25 nanoparticles/P25 nano-agglomerates in the films, three-dimensional AFM images of the TiO_2–P25 composite films without and with Tween 20 were obtained and are shown in Fig. 4(a) and (b). It can be clearly seen that the size of the aggregates at the surface of TiO_2–P25 composite films obtained in the absence of Tween 20 is larger than that of TiO_2–P25 films prepared in the presence of Tween 20. These results show that adding Tween 20 into the sol is beneficial to the improvement of the dispersion of P25 nanoparticles/P25 nano-agglomerates and the decrease in aggregate size. Therefore, the structural integrity of TiO_2–P25 composite films can be improved by incorporating Tween 20 in the sol. Enhanced dispersion of P25 nanoparticles/P25 nano-agglomerates in the film may be due to (1) enhanced viscosity of the titania sol, which is beneficial to the enhancement in skin friction resistance of P25 nanoparticles during their Brownian motion and gravity settling in the sol, which in turn can inhibit further coagulation of P25 nanoparticles, and (2) P25 nanoparticles may be stabilized by Tween 20 due to its hydrophobic interaction with the P25 nanoparticles in the sol [46]. Although increasing Tween 20 loading can increase film thickness (refer to Table 2), the tape test showed that good adhesion between the films and the borosilicate glass could be maintained at Tween 20 loading up to 50% (v/v) in the final sol. Therefore, considering also the mechanical stability of these films, this content was selected as optimum.

3.3. Optical properties

UV–vis spectroscopy was employed to obtain information on the optical properties of TiO_2–P25 composite films prepared at

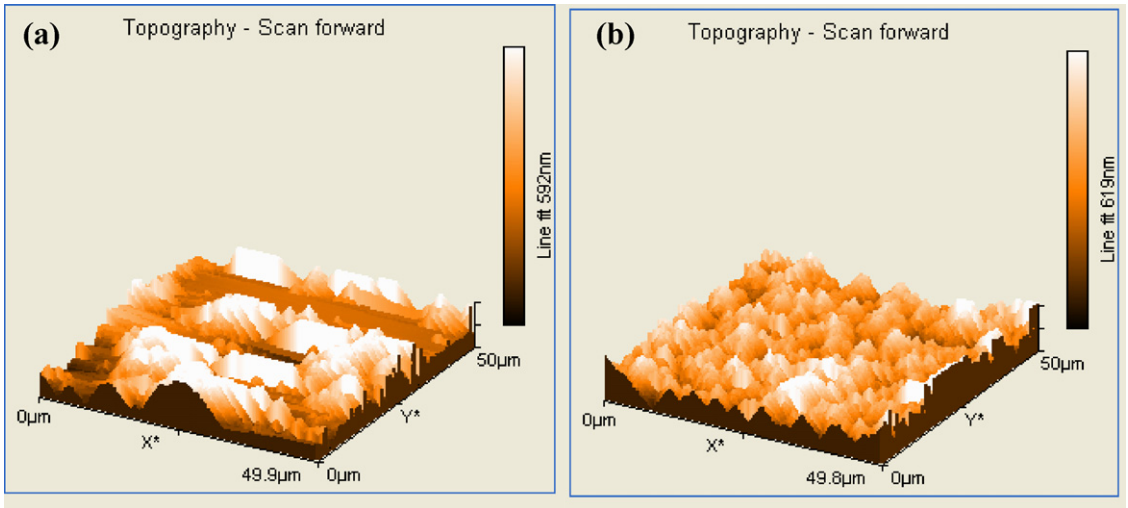

Fig. 4. Three-dimensional AFM images of TiO_2–P25 composite films (one dip-coating layer). (a) Without Tween 20 and (b) Tween 20: final sol = 1:2 (v/v).

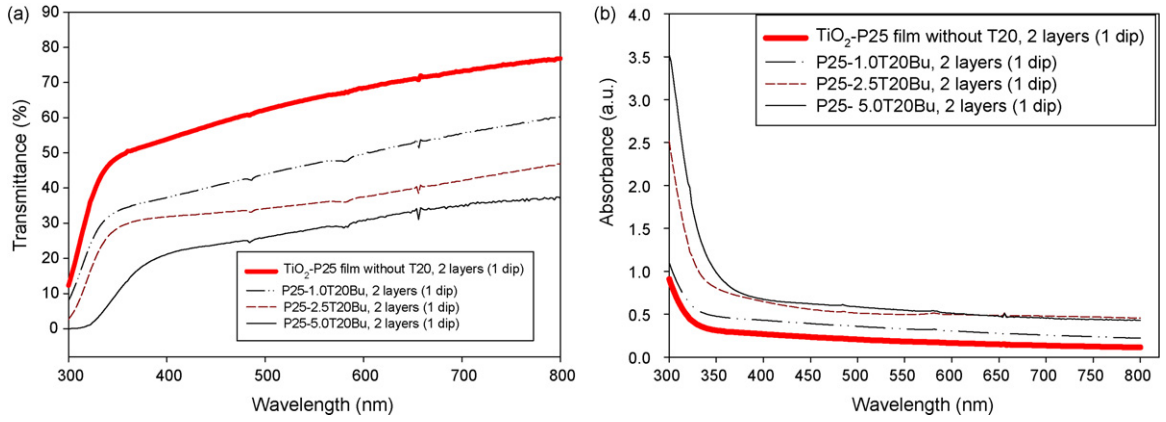

Fig. 5. UV–vis spectra of photocatalytic films with different Tween 20 loading. (a) Transmittance of TiO_2–P25 composite films and (b) absorbance of TiO_2–P25 composite films.

different Tween 20 loadings. The results are shown in Fig. 5. For the UV–vis spectroscopy analysis, the borosilicate glass was used as a blank. The results showed that increasing Tween 20 loading leads to an enhancement in the absorbance of TiO_2–P25 composite films at the wavelength range from 300 to 800 nm. Among many factors, such as film thickness, porosity, and crystalline composition, which affect the transmittance/absorbance of photocatalytic films [47], the increase in film thickness with increasing Tween 20 loading is believed to be the main factor contributing to the increase in absorbance of the TiO_2–P25 composite film. From Fig. 5(b), it can also be noted that increasing Tween 20 loading can lead to a slightly pseudo red shift of the absorption edge in the films. This is most probably due to the increase of the level of remaining organic impurities (i.e., carbon residues after calcination) with increase in Tween 20 loading. Unlike most transparent TiO_2 films [28], which have oscillation in their UV transmittance curve, there was no oscillation for the TiO_2–P25 composite films. This is attributed to several factors, such as the difference in their light scattering, film thickness [28], crystallite size, and phase structure [48].

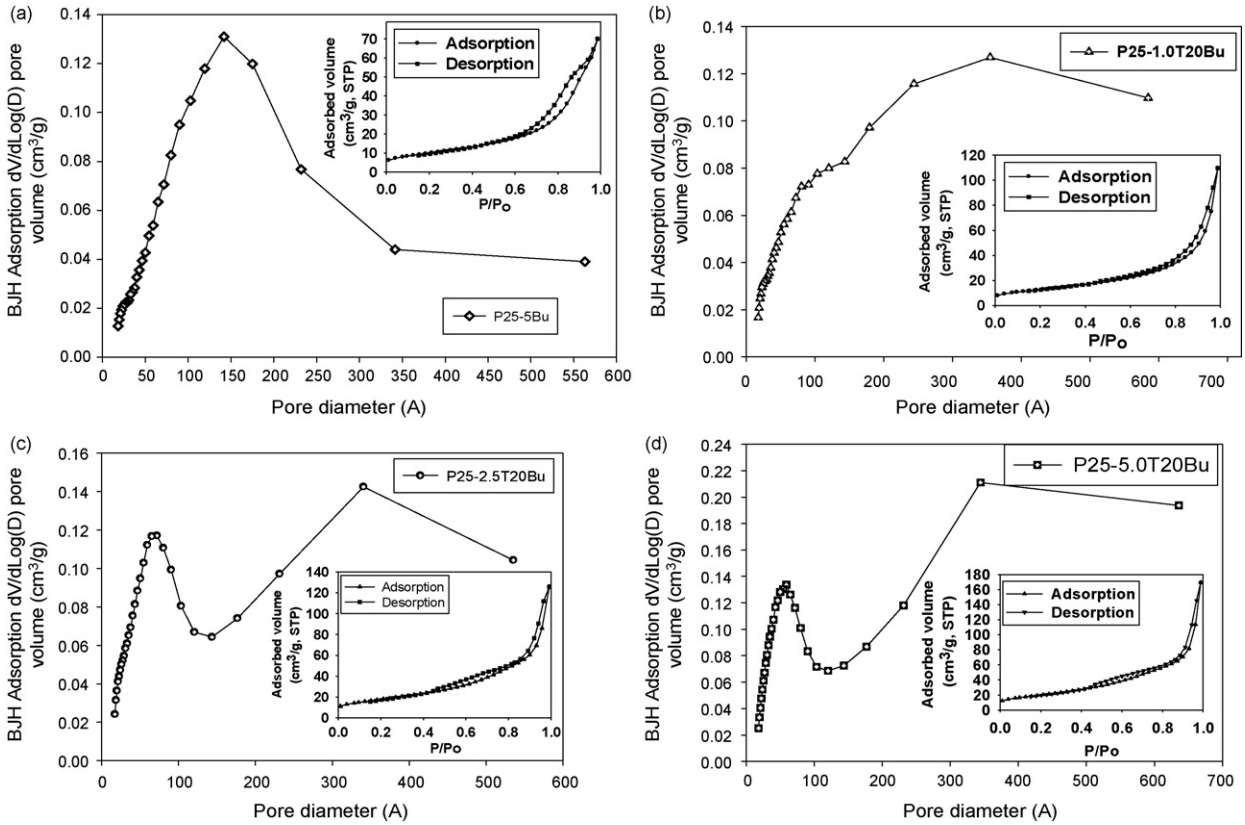

Fig. 6. Pore size distribution of TiO_2–P25 composite films. (a) No Tween 20, (b) Tween 20: final sol = 1:10 (v/v), (c) Tween 20: final sol = 1:4 (v/v), and (d) Tween 20: final sol = 1:2 (v/v). The inserted graph is the adsorption isotherm of each film.

3.4. Textural structure of the films

In order to investigate how Tween 20 affects the textural properties of the TiO_2–P25 composite films, TiO_2 particle samples scratched from the as-prepared TiO_2–P25 composite films were analyzed by N_2 adsorption; the results are shown in Fig. 6(a)–(d) and summarized in Table 2. It was found that increasing Tween 20 loading in the P25 powder-modified sol could not only lead to an obvious enhancement in the BET surface area and pore volume/porosity of the films, but also to an evolution of pore structure from mono-modal pore size distribution to bimodal pore size distribution. The inserted adsorption isotherms in Fig. 6(a)–(d) show that all photocatalytic films presented type IV isotherms, which suggested that there is mesoporous structure in these films [49]. The hysteresis loop of TiO_2–P25 composite film without Tween 20 addition (P25–Bu) exhibited a type of mixture of H2 at lower relative pressure and H3 at higher relative pressure, while those of TiO_2–P25 composite films with Tween 20 addition in the sol exhibited a type close to H3. Two major capillary condensation steps can be observed in the hysteresis loops of P25–2.5T20Bu and P25–5.0T20Bu film. The hysteresis loop at lower relative pressure region ($0.4 < P/P_0 < 0.8$) is attributed to smaller mesopore, while that at higher relative pressure ($0.8 < P/P_0 < 1.0$) is attributed to larger mesopores. Some slit-shaped pores can be observed in HRTEM images of P25–5.0Bu film and P25–5.0T20Bu film (refer to Fig. 7(a) and (b), respectively), which further proved that formation of slit-shaped pores was an important reason for the H3 type hysteresis loops [49]. Fig. 6(a) shows that P25–Bu film has the pore size of ~13 nm with the maximum pore volume. Many irregular inter-particle pores with the size near 13 nm can be seen in the HRTEM image of P25–Bu sample, which are shown in Fig. 7(a). Formation of such an irregular inter-particle pore is due to the function of the larger Degussa P25 particle as a kind of pore wall. Fig. 6(b)–(d) shows that incorporating Tween 20 into the P25 powder-modified sol can not only create smaller mesopores, but also large mesopores. As Tween 20 loading reached 50% (v/v), the film (P25–5.0T20Bu) has smaller mesopores with ~5 nm at the maximum pore volume in the small pore range and larger pore of ~34 nm at the maximum pore volume in the large pore range. Fig. 6(b) shows a transition stage in the evolution of pore structure induced by low loading of Tween 20 (Tween 20: final sol =1:10 v/v). It seems that incorporating Tween 20 into the P25 powder-modified sol can lead to the transformation of P25 particle associated inter-particle pores into larger pores. When the Tween 20 loading is high enough, such as 25% or 50% (v/v) in the P25 powder-modified sol, an obvious bimodal pore structure can be formed. Results in Fig. 6(c) and (d) show that increasing Tween 20 loading increases both smaller and larger pore volumes. Fig. 7(b) presents HRTEM image of P25–5.0T20Bu sample. Many smaller mesopores with ~5 nm and few larger irregular mesopores with ~35 nm can be observed. Interconnected smaller particles with ~8 nm should originate from TTIP hydrolysis and condensation, while larger particles with crystal size above 25 nm (i.e., 40 nm) should be Degussa P25 particles. Therefore, such a larger mesopore is associated with larger Degussa P25 particles as a kind of pore wall. Our results show that increasing Tween 20 loading in the sol without P25 particle addition cannot lead to the formation of larger mesopores or bimodal PSD [17], therefore, it is believed that the formation of more micelles induced by higher Tween 20 loading in the sol may be one of the reasons for the formation of secondary larger pores. On the other hand, although the volume and size of the larger pores are large, the average pore size of P25–1.0T20Bu, P25–2.5T20Bu and P25–5.0T20Bu is only 13.3, 10.9 and 12.2 nm, respectively (refer to Table 2). Therefore, the smaller

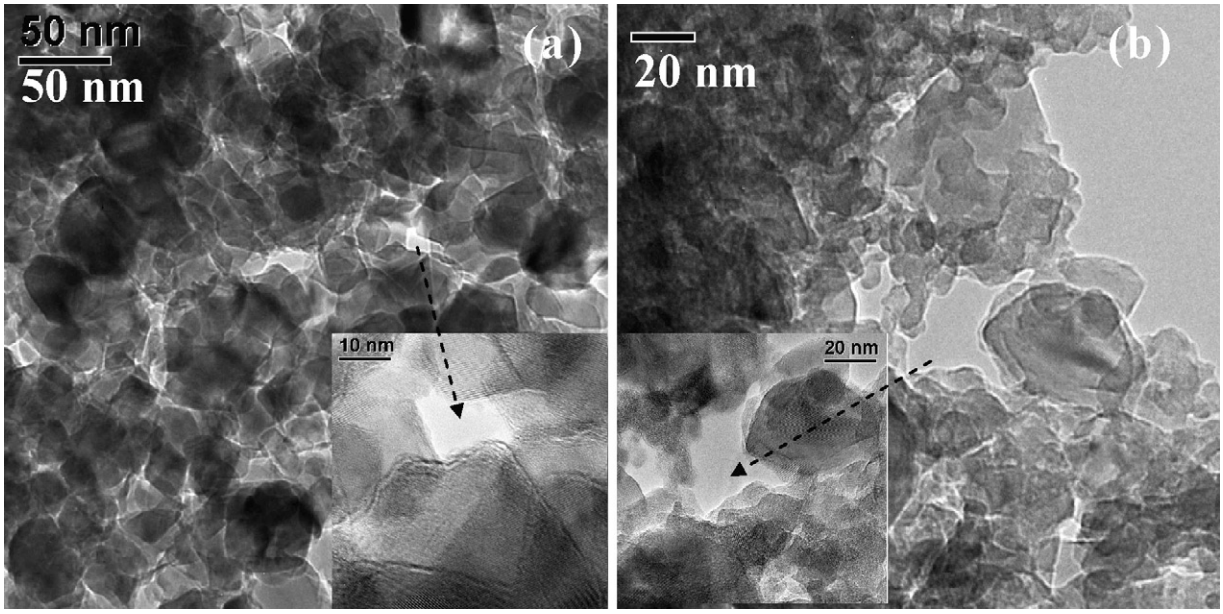

Fig. 7. HRTEM images of TiO_2–P25 composite film. (a) Crystallites and pore structure of TiO_2–P25 composite film without Tween 20 addition and (b) crystallites and pore structure of TiO_2–P25 composite film with Tween 20 addition (Tween 20: final sol = 1:2 v/v).

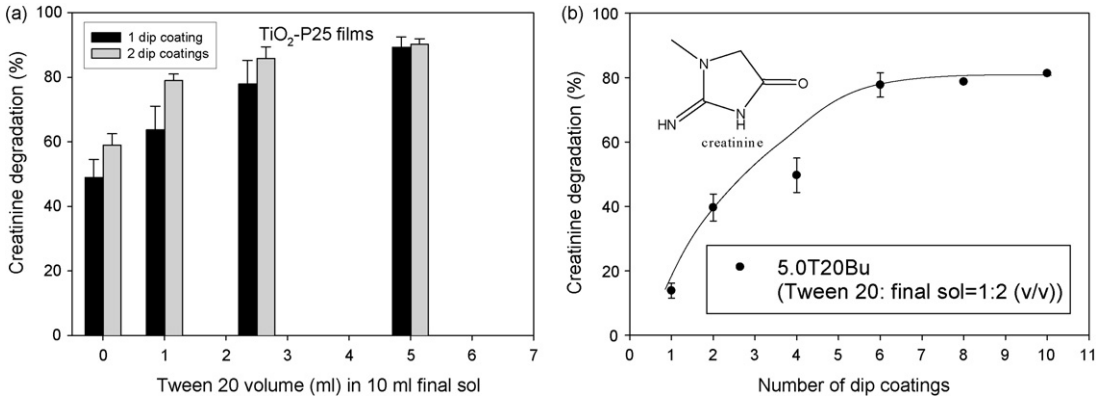

Fig. 8. (a) Photocatalytic activity of TiO_2–P25 composite films with different Tween 20 loadings and (b) photocatalytic activity of mesoporous TiO_2 film with optimum Tween 20 loading (Tween 20: final sol = 1:2 v/v) and different number of dip-coating layers).

mesopores were still a major contributor between the two types of pores. As discussed above, in this method, P25 nanoparticles/nano-agglomerates have in fact been incorporated into the framework of porous TiO_2 matrix. As a result, they function as another type of building block, which can induce the formation of secondary large mesopores. Consequently, by incorporating Degussa P25 nanoparticles into a surfactant-based sol–gel system seems to be a promising method for developing interesting architectures of bimodal mesostructured inorganic materials, which may have tailor-design properties for a variety of applications [33].

3.5. Photocatalytic degradation of creatinine in water

Creatinine is an important human metabolite present in human urine, which is also present in space wastewater [50]. Therefore, degradation of creatinine is an interesting application with respect to water purification, especially for recycling and reuse of water in space applications. Fig. 8(a) shows the degradation of creatinine by the TiO_2–P25 composite films with different Tween 20 loadings. Considering that the remaining carbon composition of organic impurities in the films was so small that they cannot be detected using energy dispersive spectroscopy (EDS) analysis (detection limit of EDS is 0.5–1 at%), it is reasonable to assume that such a small amount of residual impurities will not have a significant effect on the long-term mechanical stability of the films in water treatment applications. Control tests showed that adsorption of creatinine in the reactor vessel with these photocatalytic films was negligible and there was no obvious degradation of creatinine by photolysis alone (absence of photocatalytic films) or visible light photocatalysis after 150 min. Therefore, the decrease in the concentration of creatinine in solution is mainly due to TiO_2 photocatalysis under UV radiation.

Increasing Tween 20 loading in the sol enhances the photocatalytic activity of the TiO_2–P25 composite films, which was mainly attributed to the increase in BET surface area, pore volume, UV light utilization, and increase in the amount of crystalline materials (film weight) on the support. Fig. 8(b) shows the effect of the number of dip coatings on the photocatalytic activity of the mesoporous TiO_2 films (without P25 nanoparticles) with optimum Tween 20 loading (50% (v/v), Tween 20: final sol = 1:2 v/v). The photocatalytic degradation of creatinine by TiO_2 film at optimum preparation conditions (Tween 20: final sol = 1:2 v/v, six dip-coating layers) was only 78% after 150 min of reaction, while that of TiO_2–P25 composite film at optimum preparation conditions (Tween 20: final sol = 1:2 v/v, one dip-coating layer) was 89% and that of TiO_2–P25 composite film with Tween 20: final sol = 1:4 (v/v) at two dip-coating layers was 86% (refer to Fig. 8(a) and Table 2). Therefore, TiO_2–P25 composite films with Tween 20: final sol = 1:2 or 1:4 had higher photocatalytic activity than the mesoporous TiO_2 films. Our experimental results show that although mesoporous TiO_2 films at optimum preparation conditions (six dip-coating layers) have high transmittance (77.4%), their photocatalytic activity cannot be further improved by increasing the number of dip-coating cycles. This could be related to mass transfer limitations between creatinine and active sites in the inner layers of the mesoporous TiO_2 film with a mono-modal mesopore structure with small pore size (i.e., 5 nm).

Considering several advantageous characteristics of mesoporous TiO_2–P25 composite films such as the small number of dip coatings necessary to obtain optimum film thickness (i.e., one dip coating), relatively low amount of Tween 20 loading employed (P25–2.5T20Bu film), high UV light absorbance, large porosity, bimodal pore size distribution, and high photocatalytic activity, TiO_2–P25 composite films with Tween 20: final sol = 1:4 and 1:2 (v/v) are proved to be promising photocatalysts suitable for water purification. Because the precursor sol does not contain inorganic acid or organic acid, which is beneficial to avoiding acidic corrosion of metal supports during calcination, this method could also be promising for the immobilization of TiO_2–P25 composite films on the metal substrates (i.e., stainless steel) for water treatment and other applications.

4. Conclusions

Bimodal mesoporous TiO_2–P25 composite films can be successfully synthesized by incorporating nonionic surfactant Tween 20 as template into a P25 powder-modified sol (10 g/L

P25 nanoparticle loading). The conclusions obtained are summarized below:

1. Increasing Tween 20 loading can lead to an enhancement in BET surface area, pore volume/porosity, UV absorbance, film thickness/film weight and photocatalytic activity.
2. Tween 20 combined with 10 g/L P25 can lead to the formation of a bimodal pore size distribution. Larger Degussa P25 nanoparticles/P25 nano-agglomerates can function as a kind of pore wall contributing the formation of the secondary large mesopore.
3. Compared with the TiO_2–P25 film without Tween 20 addition, adding Tween 20 into the P25 powder-modified sol is beneficial to the decrease in crack formation due to decreased degree in the coagulation of dispersed P25 nanoparticles/P25 nano-agglomerates in the sol.
4. The TiO_2–P25 composite films with Tween 20: final sol = 1:2 (v/v) (one dip-coating layer) and 1:4 (v/v) (two dip-coating layers) have higher photocatalytic activity than the mesoporous TiO_2 films at optimum preparation conditions (Tween 20:final sol = 1:2 v/v, six number of dip-coating layers).

Therefore, compared with mesoporous TiO_2 films with mono-modal mesoporous structure with small pore size, bimodal mesoporous TiO_2–P25 composite films are more promising photocatalysts for water purification.

Acknowledgments

This work was funded in whole by a grant from the Office of Biological and Physical Research of the National Aeronautics and Space Administration (NASA) (NRA grant number: NAG 9-01475).

References

[1] A. Fujishima, K. Hashimoto, T. Watanabe, TiO_2 Photocatalysis—Fundamentals and Applications, BKC, Tokyo, Japan, 1999.
[2] M.R. Hoffmann, S.T. Martin, W. Choi, D.W. Bahnemann, Chem. Rev. 95 (1995) 69.
[3] R. Molinari, M. Mungari, E. Drioli, A. Di Paola, V. Loddo, L. Palmisano, M. Schiavello, Catal. Today 55 (12) (2000) 71.
[4] O. Legrini, E. Oliveros, A.M. Braun, Chem. Rev. 93 (1993) 671.
[5] A.L. Linsebigler, G.Q. Lu, J.T. Yates, Chem. Rev. 95 (1995) 735.
[6] M.A. Fox, M.T. Dulay, Chem. Rev. 93 (1993) 341.
[7] D.F. Ollis, H. Al-Ekabi (Eds.), Photocatalytic Purification and Treatment of Water and Air, Elsevier Science Publishers BV, Amsterdam, The Netherlands, 1993.
[8] M. Gratzel, Nature 414 (2001) 338.
[9] X.C. Wang, J.C. Yu, C.M. Ho, Y.D. Hou, X.Z. Fu, Langmuir 21 (2005) 2552.
[10] J.G. Yu, J.C. Yu, W.K. Ho, Z.T. Jiang, New J. Chem. 26 (2002) 607.
[11] Y.-Q. Wang, S.-G. Chen, X.-H. Tang, O. Palchik, A. Zaban, Y. Koltypin, A. Gedanken, J. Mater. Chem. 11 (2001) 521.
[12] D. Bahnemann, Solar Energy 77 (2004) 445.
[13] M. Keshmiri, M. Mohseni, T. Troczynski, Appl. Catal. B: Environ. 53 (2004) 209.
[14] G. Balasubramanian, D.D. Dionysiou, M.T. Suidan, I. Baudin, J.-M. Laîné, Appl. Catal. B: Environ. 47 (2004) 73.
[15] E. Pelizzetti, C. Minero, Electrochim. Acta 38 (1993) 47.
[16] D.-W. Lee, S.-J. Park, S.-K. Ihm, K.-H. Lee, Chem. Mater. 19 (2007) 937.
[17] Y.J. Chen, E. Stathatos, D.D. Dionysiou, Surf. Coat. Technol., in press, corrected proof, available online 30 August 2007.
[18] J. Shang, W. Li, Y. Zhu, J. Mol. Catal. A: Chem. 202 (2003) 187.
[19] Y.J. Chen, D.D. Dionysiou, Appl. Catal. B: Environ. 69 (2006) 24.
[20] G. Balasubramanian, D.D. Dionysiou, M.T. Suidan, V. Subramanian, I. Baudin, J.-M. Laîné, J. Mater. Sci. 38 (2003) 823.
[21] Y.J. Chen, D.D. Dionysiou, J. Mol. Catal. A: Chem. 244 (2006) 73.
[22] H. Choi, E. Stathatos, D.D. Dionysiou, Appl. Catal. B: Environ. 63 (2006) 60.
[23] J.C. Yu, L. Zhang, J. Yu, Chem. Mater. 14 (2002) 4647.
[24] J.C. Yu, L. Zhang, Z. Zheng, J. Zhao, Chem. Mater. 15 (2003) 2280.
[25] Y.J. Chen, D.D. Dionysiou, Appl. Catal. A: Gen. 317 (2007) 129.
[26] Y.J. Chen, D.D. Dionysiou, Appl. Catal. B: Environ. 62 (2006) 255.
[27] H. Choi, E. Stathatos, D.D. Dionysiou, Thin Solid Films 510 (2006) 107.
[28] J.C. Yu, J.G. Yu, J.C. Zhao, Appl. Catal. B: Environ. 36 (2002) 31.
[29] A. Mills, G. Hill, S. Bhopal, I.P. Parkin, S.A. O'Neill, J. Photochem. Photobiol. A: Chem. 160 (2003) 185.
[30] S. Ngamsinlapasathian, S. Sakulkhaemaruethai, S. Pavasupree, A. Kitiyanan, T. Sreethawong, Y. Suzuki, S. Yoshikawa, J. Photochem. Photobiol. A: Chem. 164 (2004) 145.
[31] S. Ngamsinlapasathian, T. Sreethawong, Y. Suzuki, S. Yoshikawa, Sol. Energy Mater. Sol. Cells 86 (2005) 269.
[32] J.H. Sun, Z.P. Shan, T. Maschmeyer, J.A. Moulijn, M.-O. Coppens, Chem. Commun. (2001) 2670.
[33] P.D. Yang, T. Deng, D.Y. Zhao, J.L. Feng, D. Pine, B.F. Chmelka, G.M. Whitesides, G.D. Stucky, Science 282 (1998) 2244.
[34] Z.Y. Yuan, J.L. Blin, B.L. Su, Chem. Commun. (2002) 504.
[35] T. Klimova, E. Carmona, J. Ramirez, J. Mater. Sci. 33 (1998) 1981.
[36] L. Wu, J.C. Yu, X.C. Wang, L.Z. Zhang, J.G. Yu, J. Solid State Chem. 178 (2005) 321.
[37] A. Vantomme, A. Léonard, Z.Y. Yuan, B.L. Su, Colloid Surf. A: Physicochem. Eng. Aspects 300 (2007) 70.
[38] Y. Zhang, M. Koike, N. Tsubaki, Catal. Lett. 99 (2005) 193.
[39] O. Levenspiel, Chemical Reaction Engineering, 2nd ed., Wiley, New York, 1972, p. 496.
[40] American Society for Testing and Materials, ASTM, West Conshohocken, PA, D-3359-02 cross-cut tape test for adhesion.
[41] A.K. Dash, A. Sawhney, J. Pharm. Biomed. Anal. 29 (2002) 939.
[42] M.G. Antoniou, U. Nambiar, D.D. Dionysiou, Catal. Today 124 (2007) 215.
[43] R.K. Iler, The Chemistry of Silica: Solubility, Polymerization, Colloid and Surface Properties and Biochemistry, John Wiley & Sons, New York, 1979.
[44] C.J. Brinker, G.W. Scherer, Sol–Gel Science—The Physics and Chemistry of Sol–Gel Processing, Academic Press, San Diego, 1990.
[45] S. Ardizzone, C.L. Bianchi, G. Cappelletti, Surf. Interf. Anal. 38 (2006) 452.
[46] N.H. Tkachenko, Z.M. Yaremko, C. Bellmann, M.M. Soltys, J. Colloid Interf. Sci. 299 (2006) 686.
[47] A. Mills, G. Hill, M. Crow, S. Hodgen, J. Appl. Electrochem. 35 (2005) 641.
[48] J.G. Yu, J.F. Xiong, B. Cheng, S.W. Liu, Appl. Catal. B: Environ. 60 (2005) 211.
[49] S.J. Gregg, K.S.W. Sing, Adsorption Surface Area and Porosity, 2nd ed., Academic Press Inc., London, 1982.
[50] C.L. Pederson, Y. Yoon, R.M. Lueptow, in: Proceedings of the 43rd AIAA Aerospace Sciences Meeting and Exhibit, Reno, Nevada, January 10–13, 2005.